TISSUE ENGINEERING: Part C
Volume 29, Number 10, 2023

DOI: 10.1089/ten.tec.2023.0064

termis
Tissue Engineering
& Regenerative Medicine
International Society





# Evaluation of Porcine Psoas Major as a Scaffold Material for Engineered Heart Tissues

Shi Shen, PhD,[1,*] Stephanie Shao,[1,*] Maria Papadaki, PhD,[2]
Jonathan A. Kirk, PhD,[2] and Stuart G. Campbell, PhD[1,3]

Decellularized porcine myocardium is commonly used as scaffolding for engineered heart tissues (EHTs). However, structural and mechanical heterogeneity in the myocardium complicate production of mechanically consistent tissues. In this study, we evaluate the porcine psoas major muscle (tenderloin) as an alternative scaffold material. Head-to-head comparison of decellularized tenderloin and ventricular scaffolds showed only minor differences in mean biomechanical characteristics, but tenderloin scaffolds were less variable and less dependent on the region of origin than ventricular samples. The active contractile behavior of EHTs made by seeding tenderloin versus ventricular scaffolds with human-induced pluripotent stem cell-derived cardiomyocytes was also comparable, with only minor differences observed. Collectively, the data reveal that the behavior of EHTs produced from decellularized porcine psoas muscle is almost identical to those made from porcine left ventricular myocardium, with the advantages of being more homogeneous, biomechanically consistent, and readily obtainable.

**Keywords:** tissue engineering, decellularized scaffolds, engineered heart tissue, cardiomyocyte, stem cell

### Impact Statement

We evaluated decellularized porcine psoas muscle as a novel alternative to decellularized porcine myocardium as a scaffold for engineered heart tissue (EHT) formation. Scaffolds produced from decellularized porcine psoas muscle yielded EHTs that were essentially indistinguishable from those made from decellularized myocardial tissue in terms of muscle contraction, while offering significant benefits such as ease of procurement, material consistency, and cost.

## Introduction

Three-dimensional engineered heart tissues (EHTs) are created by combining cardiac cells with an extracellular matrix (ECM) material to serve as a scaffolding substrate. Various native and synthetic biomaterials have been used to mimic the native cardiac tissue environment to produce functional contractile tissues.[1] Decellularized tissues[2] and whole hearts[3,4] from porcine or human cadavers have been used as scaffolds for EHT creation owing to their ability to impart realistic ECM composition, microstructure, and material properties. Decellularization involves the complete removal of all the cells originally present in the native tissues, leaving an intact ECM structure ready for the reintroduction of autologous or allogeneic cells.

[1]Department of Biomedical Engineering, Yale University, New Haven, Connecticut, USA.
[2]Department of Cell and Molecular Physiology, Loyola University Stritch School of Medicine, Maywood, Illinois, USA.
[3]Department of Cellular and Molecular Physiology, Yale University, New Haven, Connecticut, USA.
*These authors contributed equally to this work.

Common means of decellularization involve chemical, biological, or physical agents or processes,[5–7] with chemical detergents such as sodium dodecyl sulfate (SDS) being most common.[8] Since the removed cells are the main source of potential host immune response for transplant or regenerative applications, this approach offers the advantage of a favorable natural environment for cardiac cells without immunogenic concerns.[4] Moreover, decellularized ECMs retain highly similar passive mechanical profiles to native tissues.[9,10] Combined with the versatility and virtually unlimited quantity of human-induced pluripotent stem cell-derived cardiomyocytes (hiPSC-CMs),[11] these scaffolds can serve as the basis for disease modeling,[12,13] tissue and cellular mechanics studies,[14] and drug screening.[15]

Given the general lack of availability and limited quantities of human tissues for decellularized scaffolds,[16] xenogeneic cardiac tissue scaffolds made from available animal hearts (porcine in particular) are commonly used. Besides the inherent lack of immunogenicity after decellularization, porcine heart offers highly similar anatomical and physiological features to human hearts.[17] With the first porcine heart transplant recently completed,[18] porcine tissues may be more commonly used in EHTs *in vitro* and as xenogeneic or semixenogeneic materials in the clinical setting.[19]

Still, decellularized porcine cardiac tissue has some drawbacks as a source of scaffolding for EHTs. Specifically, the muscle fiber orientation varies significantly from endocardium to epicardium in the myocardium, and the ratio of circumferential fibers to fibers oriented longitudinally also changes from the base to the apex.[20,21] When cutting slices of ventricular tissue to use for EHT scaffolding, significant structural and mechanical variations can occur among ECM scaffolds from the same heart, simply because they are cut from different regions. Since EHTs may already face variable degrees of cell attachment and survival compared to the actual heart,[4] further variability only serves to complicate the consistency and quality of EHTs, diminishing their potential as a tool for *in vitro* and translational research.

We hypothesized that the porcine psoas major muscle (tenderloin) could be an alternative source of xenogeneic decellularized ECM scaffold, providing a more consistent and convenient material source than myocardial tissue. Porcine psoas major is a skeletal muscle that runs adjacent to the central portion of the spine. Since it is used for posture instead of locomotion, it has the lowest fat content compared with any major muscle.[22] Moreover, skeletal muscles tend to maintain uniform structural and histochemical properties along their entire length, unlike the myocardium.[23]

As a result, combined with the tenderloin's unique location and uniform cylindrical shape, we hypothesize that porcine tenderloin may possess more structurally consistent decellularized ECM for making EHTs. If this holds true, porcine tenderloin may serve as a more consistent scaffold material with potentially greater accessibility and yield for cardiac tissue engineering. In this study, we compared the biomechanical and biochemical composition, the degree of variation, and the physiological behavior of EHTs made from either porcine myocardial or psoas-derived decellularized tissue scaffolds.

## Methods

### Materials

Dulbecco's modified Eagle's medium (DMEM), Dulbecco's phosphate-buffered saline (DPBS), RPMI 1640 medium, fetal bovine serum (FBS), penicillin-streptomycin (P/S, 10,000 U/mL), B-27 supplements with and without insulin, non-essential amino acids (NEAA), L-glutamine, sodium pyruvate, goat serum, mouse anti-Collagen type I antibody (MA1-26771), goat anti-mouse Alexa Fluor 488 secondary antibody, and ProLong diamond antifade mountant with DAPI were purchased from Thermofisher Scientific. Pluronic F-127 came from Sigma Aldrich. mTESR media, CHIR99021, and IWP4 were from Stemcell Technologies.

### Tissue procurement, processing, and cryostat sectioning

Both porcine heart and tenderloin (psoas major) were obtained the day after slaughter from the same 10–11-month-old herd (Provisions on State, New Haven, CT). After purchase, both the heart and the tenderloin were immediately submerged in ice-cold DPBS with 5% Penicillin-Streptomycin for transport. For heart processing, a surgical scalpel was used to trim away the atria and right ventricle, leaving only the left ventricle (LV). The LV was cut from the base end to the apex so it could be flattened into a roughly rectangular block. Endocardial and epicardial portions of the LV were then removed.

The LV free wall was cut into 3-cm square blocks, and these were flash frozen on crushed dry ice and stored in a −80°C freezer. For tenderloin processing, the muscle and connective tissues surrounding the tenderloin longitudinal midsection were trimmed off with a scalpel. The midsection portion was further trimmed and cut into 3-cm square blocks, flash frozen on dry ice, and stored in a −80°C freezer. LV blocks were divided and labeled into three regions from the base to the apex, and tenderloin blocks were divided into three regions lying sequentially along the longitudinal axis of the muscle.

A cryostat microtome (Leica CM3050 S) was used to section LV blocks into 150-μm-thick longitudinal slices. The block was mounted onto the sample disk with Tissue-Tek compound (Sakura) at −13°C object temperature. A low-profile diamond microtome blade was used to cut the block at a 7.5-degree angle. Once cut, the slices were labeled and stored in a large Petri dish in the −80°C freezer.

### Maintenance and differentiation of hiPSC-CMs

This study used an existing human induced pluripotent stem cell line and hence did not require IRB approval. A healthy control stem cell line (GM23338; Coriell Institute) was cultured in mTESR until close to 100% confluency. A commonly used differentiation protocol was followed to produce ventricular cardiomyocytes.[11] On day 0, 15 μM CHIR99021 was added for 24 h, and 5 μM IWP4 was added in media on day 3 for 48 h. Cells were cultured in RPMI with B-27 minus insulin supplement until day 9. Afterward, RPMI with B-27 plus insulin was used. A 4-day cardiomyocyte purification process was initiated on day 12 with 4 mM lactate in RPMI without glucose. Cells were used for EHT seeding on day 18.

### *Fabrication, seeding, and maintenance of EHTs*

To produce EHTs, frozen LV and tenderloin slices were laid flat on top of cover glass slides (25 mm diameter; Bellco Glass) held in a 3D printed cover glass holder. Slices were then laser cut into $2.5 \times 6$ mm rectangular strips and submerged in DPBS. The strips were incubated in lysis buffer with 10 mM Tris and 0.1% 0.5 M EDTA for 2 h. EHT holders were prepared from 0.1-inch-thick Teflon PTFE sheets (ePlastics). After laser cutting, EHT Teflon holders were cleaned and autoclaved before scaffolds were fixed onto the EHT holders. Assembled scaffolds were decellularized in 0.5% wt/vol SDS in DPBS for 30 min at 50 RPM on a plate shaker. Finally, the scaffolds were incubated overnight in an incubation media (DMEM, 10% FBS, and 2% P/S) before seeding.

For EHT seeding, hiPSC-CMs were dissociated with TrypLE and adult human cardiac fibroblasts (aHCFs, 306-05A; PromoCell) were thawed from liquid nitrogen storage. A total of one million cells were seeded onto each tissue, with 90% hiPSC-CMs and 10% aHCFs. Seeding media were made ahead of time with DMEM, 10% FBS, 1% P/S, 1% NEAA, 1% L-glutamine, and 1% sodium pyruvate. After seeding, the tissues were maintained in DMEM supplemented with B-27 plus insulin. Media were changed every other day. The tissues were monitored for 2 weeks to allow proper cell attachment and contractile synchronization before experiments.

### *Mechanical testing and data analysis*

A custom setup was used to characterize the biomechanical properties of EHTs. The system comprised a pair of linear actuators and a force transducer to measure the mechanical behavior of scaffolds or tissues in real time. A custom 3D printed bath surrounded with heating elements, thermistor probe, and a pair of platinum wires enabled the tissues to be studied at physiological temperature, under controlled electrical stimulation frequency and continuous superfusion of Tyrode's solution.

Tyrode's solution was freshly prepared for every experiment (in mM: 140 NaCl, 5.4 KCl, 1.8 $CaCl_2$, 1 $MgCl_2$, 25 HEPES, and 10 glucose; pH 7.3). A custom application written in MATLAB (Natick, MA) in conjunction with a PC-based data acquisition system (Microstar Laboratories, Bellevue, WA) was used for system control, data recording, and analysis. Optical coherence tomography (Thorlabs) was used to measure the tissues' cross-sectional areas for mechanical data normalization. GraphPad Prism 9 was used for statistical analysis and data visualization.

### *Immunohistochemistry*

LV and tenderloin scaffolds were first fixed in formalin for 15 min in the chemical hood and washed with DPBS thrice. The fixed scaffolds were then permeabilized in 0.1% Triton X-100 for 10 min, and blocked in DPBS with 5% goat serum for 1 h. For primary antibody staining, the samples were incubated overnight in DPBS with 0.05% Tween-20 and collagen type I antibody at 1:2000 in the 4°C fridge. One hour before imaging, the samples were incubated in DPBS with the Alexa Fluor 488 secondary antibodies covered with aluminum foil in room temperature. For imaging, samples were mounted with Prolong diamond antifade mountant with DAPI, and images were taken with a fluorescence microscope camera (LEICA DFC9000) and processed in LAS X (LEICA) and ImageJ.

### *Mass spectrometry*

Mass spectrometry ECM samples were prepared as stated previously, except the samples were amply decellularized for 60 min to confirm there would be no remaining cellular protein that could interfere.[24,25] After the decellularization process, the tissue was homogenized and sonicated in 4 M GnHCl, 50 mM sodium acetate, pH 5.8, and protease inhibitors (Fisher Scientific) after washing twice with deionized water. The samples were maintained for 70 h in this buffer at room temperature, with agitation for 15 s at 1000 RPM every 30 s.

The samples were then centrifuged at 4000 RPM for 25 min at 4°C, the supernatant was removed and stored at −80°C, and the pellets were resuspended in de-glycosylation buffer (150 mM NaCl, 50 nM sodium acetate, pH 6.8 and protease inhibitors) and 0.05 U of each of the following enzymes: chondroitinase ABC from Proteus vulgaris (Sigma), endo-β-galactosidase from Bacteroides fragilis (Sigma), and heparinase II from Flavobacterium heparinum (Sigma) and incubated overnight at 37°C with agitation.

The remaining pellet was solubilized with 20 μL DMSO and the samples were pooled together with the supernatant from the previous step to combine all insoluble proteins into one fraction. The sample was then prepared for in-solution digestion for mass spectrometry in the following way: Four volumes of prechilled acetone were added to the sample and incubated for 30 min at −20°C. After centrifugation for 10 min at 15,000 *g* at 4°C, the supernatant was removed and the pellet was resuspended with 70% acetone and centrifuged again. The supernatant was removed and the pellet was resuspended in 8 M urea and 400 mM ammonium bicarbonate. Reduction was performed by incubating with 500 mM DTT (1:25 v/v) at 95°C for 10 min and alkylation by incubating with 100 mM iodoacetamide (1:2 v/v) at room temperature for 30 min.

The sample was diluted $8\times$ with deionized water and digested with 1:20 w/w trypsin/Lys-C (Thermo Scientific) for 16 h at 37°C. Before mass spectrometry, the samples were cleaned up using C18 spin columns (Pierce) according to the manufacturer's instructions. Two hundred nanograms of peptides in 0.1% formic acid was loaded onto an UltiMate 3000 nanoHPLC coupled to an LTQ Orbitrap XL (Thermo). MS data analysis was performed using the Peaks Bioinformatics Software (version 8.5), where acquired masses were searched against the Sus scrofa database (SwissProt). The precursor ion mass tolerance was set at 20 ppm, the MS/MS fragment mass error tolerance was set at 1.0 kDa, and the False Discovery Rate (FDR) was set to 4%.

## Experiment

To assess and compare the structural consistency of the decellularized porcine heart tissue and tenderloin, fresh porcine heart and tenderloin from the same herd of 10–11-month-old pigs were obtained the day after slaughter. After processing, frozen left ventricular (LV) and tenderloin

blocks were further cryosectioned, laser cut, decellularized, and finally assembled into individual EHTs (Fig. 1A) as previously reported.[2] Both passive and active mechanical properties of decellularized EHT scaffolds and EHTs seeded with hiPSC-CMs were characterized, including systolic peak force and kinetic parameters (time to peak [TTP] and time to 50% relaxation, Fig. 1B). Tissue passive force (Fig. 1C), cross-sectional area (Fig. 1D), passive stress, and its derivative stiffness (Fig. 1E) were also examined.

To examine the variability in passive mechanical profiles of LV and tenderloin scaffolds, EHTs were produced from different tissue blocks. For LV, three free-wall regions were sampled from the base to the apex (LV1-LV3, Fig. 2A). Similarly, three mid-section regions from tenderloin were sampled along the length of the muscle (T1–T3, Fig. 2B). EHT fabrication and decellularization protocols remained the same for both LV and tenderloin scaffolds.

Empty, unseeded decellularized scaffolds were characterized mechanically in the same physiological testing conditions as live tissue experiments. Scaffolds from the three LV regions showed highly significant differences in passive stress across −10% to 10% stretch intervals, with LV1 (toward the base of the heart) having the lowest stress and LV3 near the apical end showing the highest passive stress (Fig. 2C). In comparison, passive stress curves of scaffolds from the three regions of the tenderloin overlapped each other and showed no significant difference (Fig. 2D).

To analyze the passive stress-strain profiles more closely, an exponential curve was fit to each specimen according to $\sigma = Ce^{k\alpha}$, where $\alpha$ represents strain, $C$ is a scaling constant, and $k$ is an exponential term representing strain dependence, and $\sigma$ being passive stress. For LV, $k$ in the LV3 group was significantly higher than in LV1 and LV2 (Fig. 2E). Meanwhile, the $k$ values for T1, T2, and T3 were again similar and showed no statistical difference (Fig. 2F).

Moreover, LV scaffold stiffness showed significant differences, with LV1 having the lowest and LV3 the highest passive stiffness across the 0% to 8% stretch (Fig. 2G). As for the tenderloin, the three groups exhibited limited and statistically insignificant deviations in stiffness (Fig. 2H). Finally, to further examine the difference in the empty EHT scaffolds, the two most consistent region materials in passive mechanics from the two (LV1 and T1) were used for immunohistochemistry (IHC). After staining for collagen at 10× magnification, LV1 scaffolds not only showed areas of significant alignment for the collagen fibers but also areas with highly disorganized fiber orientations (Fig. 2I). In contrast, collagen fiber alignment in the longitudinal direction for T1 scaffolds was consistently uniform (Fig. 2J).

Next, the active mechanical profiles of iPSC-CM-seeded LV and tenderloin scaffolds were compared. Based on the results from the previous experiment, hiPSC-CMs and adult cardiac fibroblasts were seeded onto decellularized scaffolds from the most consistent LV1 and T1 regions. Biomechanical measurements were performed 1 week after seeding to allow sufficient time for adequate cell attachment and contraction synchronization. First, passive mechanical behavior (behavior during the diastolic interval) of LV1 and T1 tissues was evaluated. When paced under 1 Hz stimulation, tenderloin tissues had similar passive stress to LV tissues before ∼4% stretch. Above 4%, T1 EHTs showed a small, but significantly higher passive stress relative to LV (Fig. 3A). Meanwhile, passive tissue stiffness showed similar trends between LV1 and T1 (Fig. 3B).

When we compared the sample active twitches between LV1 and T1 at 1 Hz, very similar morphologies were observed in terms of contraction magnitude and twitch kinetics (Fig. 3C). Assessing the potential twitch differences across stimulation frequencies showed almost identical behaviors in terms of systolic peak force (Fig. 3D) and TTP

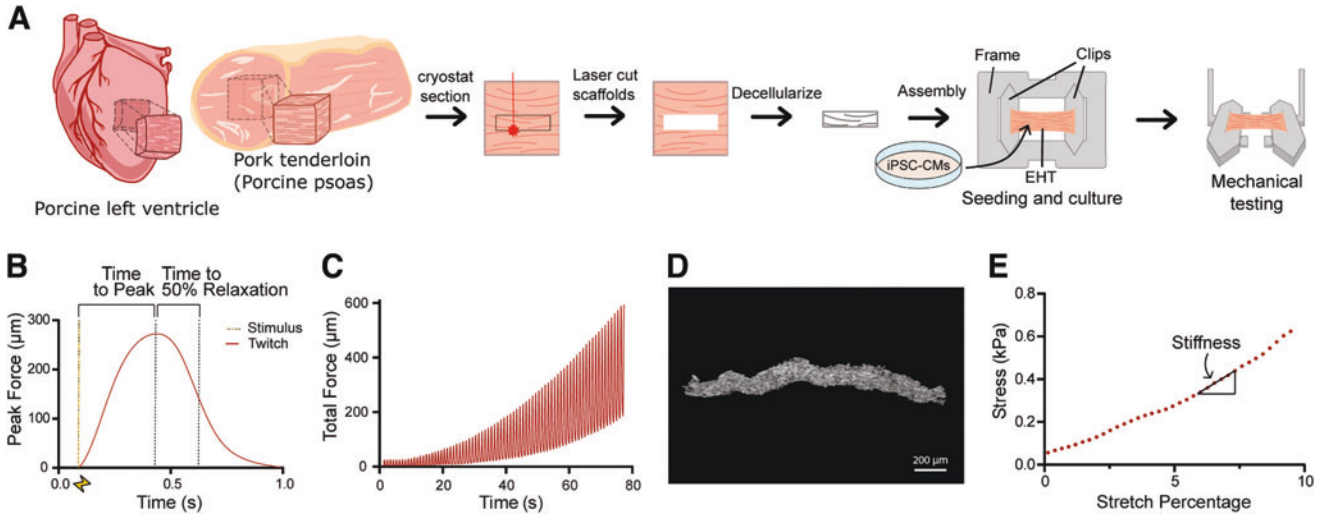


**FIG. 1.** EHT production and derivation of analytical measurements. **(A)** Porcine LV free wall is cut into 150 μm slices, from which scaffolds are laser cut. The scaffolds are decellularized, seeded with iPSC-CMs, cultured, and tested using a custom setup. **(B)** The TTP and time to 50% relaxation (RT50) are shown on the representative twitch. **(C)** Passive stress is derived by dividing the force by the cross-sectional area as the tissue is stretched from −10% to 10% stretch. **(D)** Cross-sectional area of the tissue is taken using OCT. **(E)** Stiffness is derived from the slope of the stress. TTP, time to peak; iPSC-CM, induced pluripotent stem cell-derived cardiomyocytes; EHT, engineered heart tissue; OCT, optical coherence tomography; LV, left ventricular. Color images are available online.

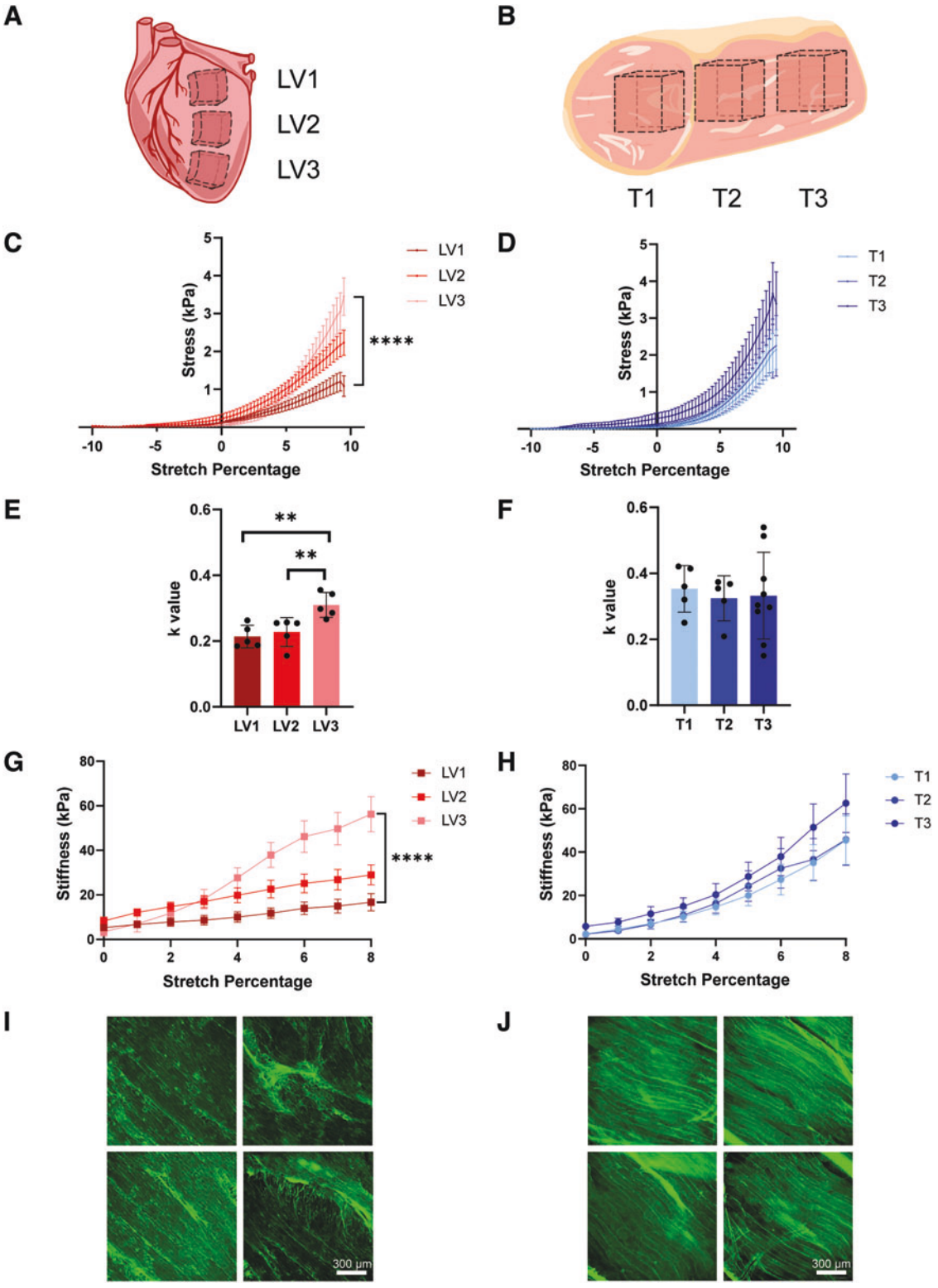


**FIG. 2.** Decellularized porcine tenderloin scaffolds are more consistent than LV scaffolds in passive mechanics. **(A)** Representation of the three different sections taken from porcine LV free wall: LV1 $n=5$, LV2 $n=5$, and LV3 $n=5$. **(B)** Representation of the three different sections taken from porcine tenderloin (T): T1 $n=5$, T2 $n=5$, and T3 $n=10$. **(C)** Passive stress mechanics of LV scaffolds being stretched from −10% to 10% ($p<0.0001$). **(D)** Passive stress of T scaffolds stretched from −10% to 10%. **(E)** LV k-values from the exponential curve fit equation $y=Ce^{ka}$ with alpha representing strain ($p=0.0034$ for LV1 vs. LV3 and $p=0.0082$ for LV2 vs. LV3). **(F)** Tenderloin passive stress exponential fit k-values. **(G)** Stiffness for LV scaffolds ($p<0.0001$). **(H)** Stiffness for T scaffolds. **(I)** Immunohistochemistry (IHC) of LV1 decellularized scaffolds staining for collagen I at 10×. **(J)** IHC of collagen-stained T1 scaffolds at 10×. Experiments were analyzed with 2-way ANOVA **(C, D, F)** with mixed effects **(G, H)** and Tukey's post hoc comparison **(E)**. $^{**}p<0.01$, $^{****}p<0.0001$. Color images are available online.

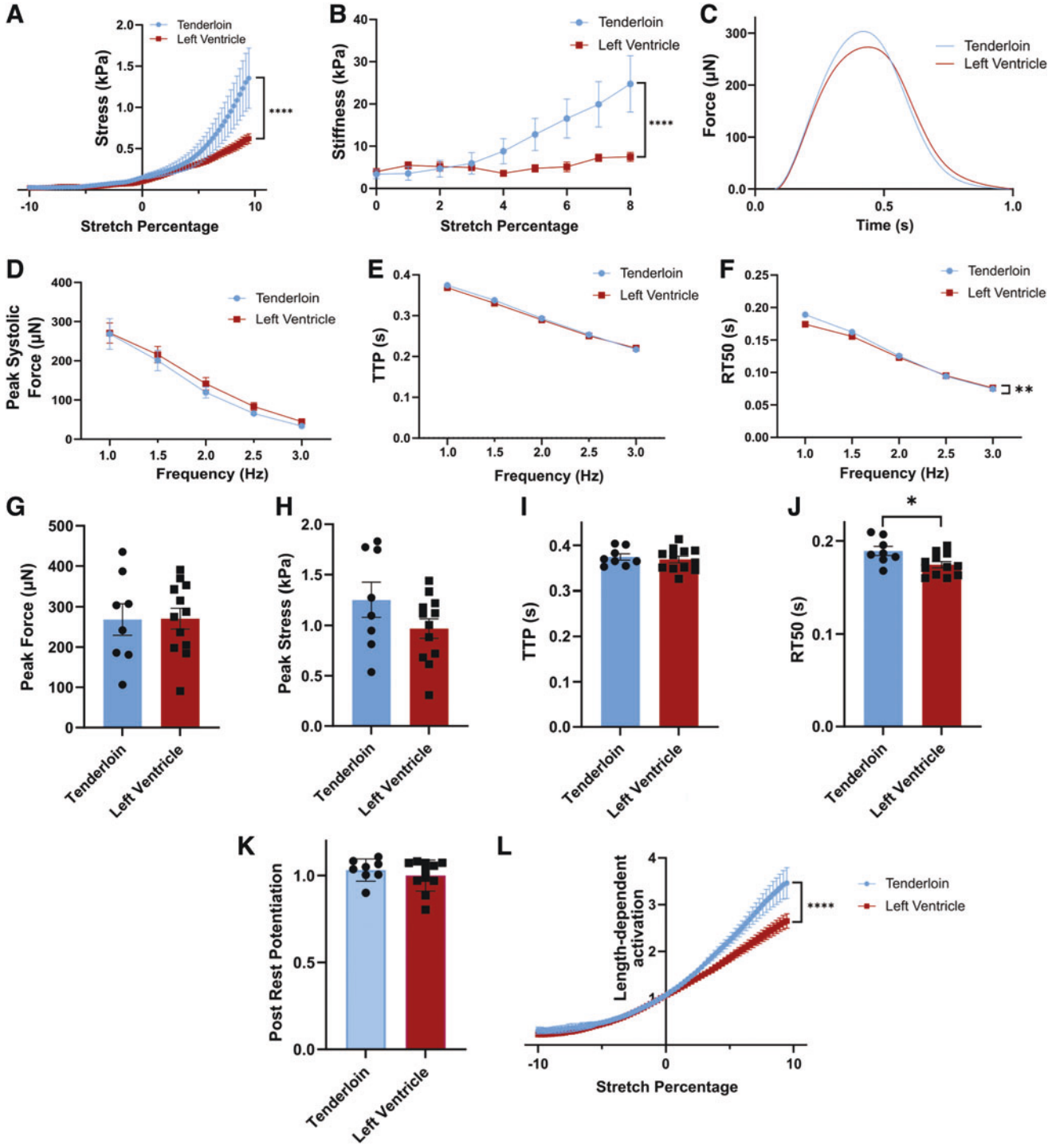


**FIG. 3.** Similar passive mechanics and active mechanics, as well as improved Frank-Starling behavior are observed in recellularized tenderloin scaffolds. Both decellularized left ventricle (LV1) and tenderloin (T1) were seeded with PGP1 iPSC-CMs and adult cardiac fibroblasts. All data were from two separate differentiation batches (LV1 $n=12$, T1 $n=8$). **(A)** Passive stress of EHTs stretched from −10% to 10% stretch (2-way ANOVA) $p<0.0001$). **(B)** Stiffness as a derivative of passive stress from culture length to 8% stretch (2-way ANOVA $p<0.0001$). **(C)** Representative force twitches of EHT at 1 Hz. **(D)** Raw peak systolic force from 1 to 3 Hz. **(E)** TTP force from 1 to 3 Hz. **(F)** Time to 50% relaxation (RT50) (2-way ANOVA with repeated measures $p=0.0057$). **(G)** Peak systolic force 1 Hz comparison. **(H)** Peak stress 1 Hz comparison. **(I)** TTP 1 Hz comparison. **(J)** RT50 1 Hz comparison ($p=0.0271$). **(K)** Postrest potentiation relationship. **(L)** Frank-Starling gain from −10% to 10% stretch. Data were analyzed using 2-way ANOVA (**A, B, D–F, L**) and unpaired two-tailed $t$ test (**G–K**). $*p<0.05$, $**p<0.01$, $****p<0.0001$. Color images are available online.

(Fig. 3E). Time to 50% relaxation showed a visible difference at 1Hz, but RT50 from both groups quickly converged after 1 Hz (Fig. 3F).

A further closer look at the active mechanics at 1 Hz again showed identical systolic peak forces (Fig. 3G), a 25% higher peak stress for tenderloin tissues after normalization (Fig. 3H), the same TTP (Fig. 3I), and marginally slower RT50 for tenderloin (Fig. 3J). Postrest potentiation, as an indirect measure of calcium handling capability of the tissues going from high-frequency pacing (3 Hz) to slow-frequency pacing (1 Hz) after a pause, showed similar limited potentiation between the two groups (Fig. 3K), indicating similar calcium reuptake performance.

The length dependence of twitch force (Frank-Starling behavior) of tissues was assessed by measuring isometric twitch force at multiple degrees of EHT stretch. LV1 and T1 tissues showed very similar length dependence below culture length, but T1 EHTs exhibited significantly higher length-dependent activation starting around 2–3% stretch (Fig. 3L).

Finally, to understand the compositional differences between tenderloin and left ventricular ECM, mass spectrometry assays were performed. Overall, total ECM protein content was marginally higher in LV, but not significant (Fig. 4A). In addition, total collagen content was similar (Fig. 4B). Within the collagen breakdown by type, tenderloin showed lower expression of type I or III, higher type IV, and similar type VI. Here, type I and type III collagen are interchangeable due to sequence homology between the two types in mass spectrometry. Next, tenderloin showed more fibrillin and Alpha-2-HS-glycoprotein, and less nidogen. As for proteoglycans, heparan sulfate proteoglycan was only expressed in LV and not in tenderloin (Fig. 4D). Finally, LV ECM had more laminin and fibronectins than tenderloin (Fig. 4E).

## Discussion

We hypothesized that decellularized porcine tenderloin ECM might serve as a more consistent scaffold material for cardiac tissue engineering than porcine left ventricular ECM, given the reported inherent fiber variability in heart muscle and reported uniformity in skeletal muscles. Through characterizing both decellularized scaffolds and recellularized EHTs, we find that tenderloin scaffolds are indeed more consistent in passive mechanical properties than LV scaffolds.

More specifically, LV scaffolds demonstrate significant variation in passive mechanics among different regions from base to apex, with higher passive stress and stiffness observed as tissue samples near the apex of the heart. Knowing that the ratio of ECM fibers aligned circumferentially to longitudinally is higher toward the base and lower near the apex,[20] apical regions may have more longitudinally directed fibers. As a result, given the passive mechanical contribution from ECM proteins, especially collagen

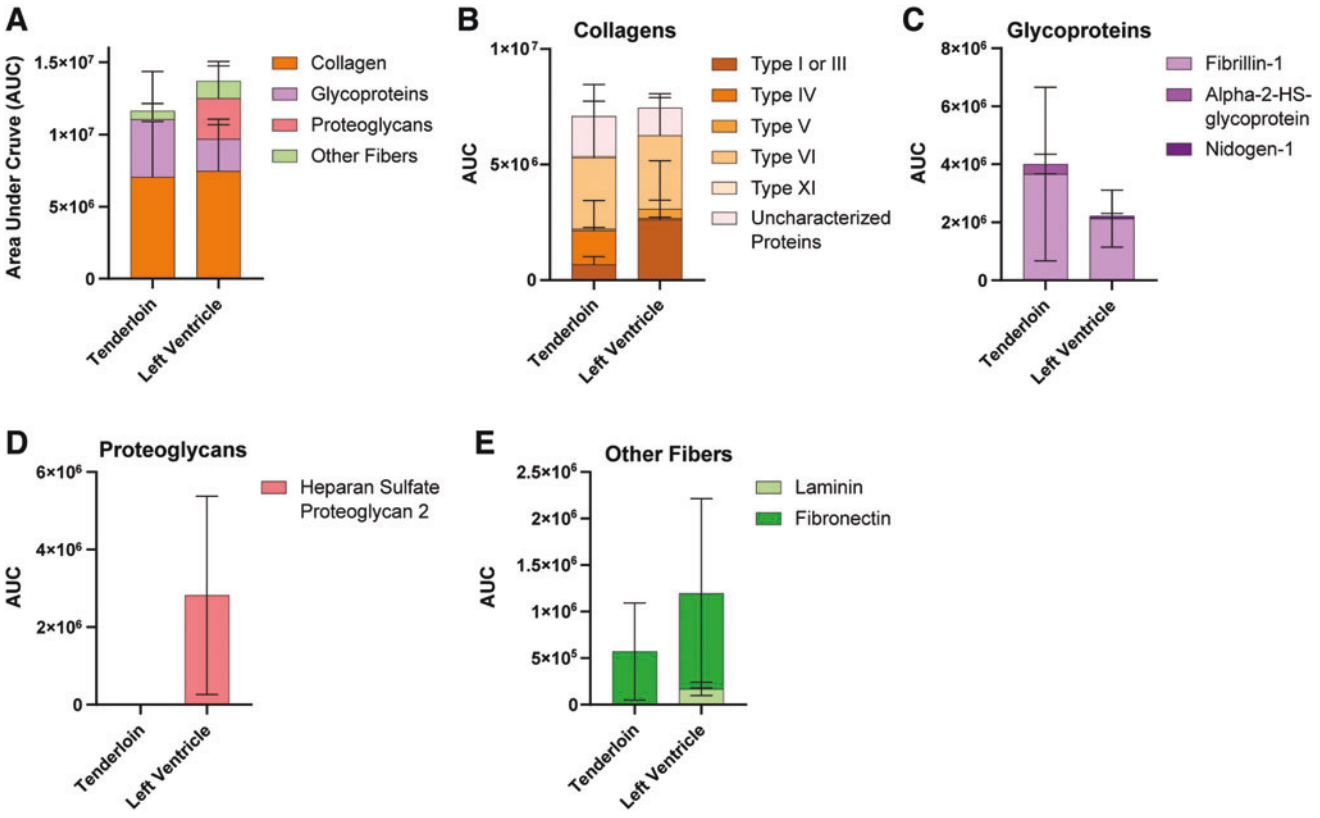


**FIG. 4.** Mass spectrometry of tenderloin and LV decellularized scaffolds shows similar composition. **(A)** Summary data of total protein and major ECM proteins in tenderloin and LV decellularized scaffolds. **(B)** Comparison of collagen composition. **(C)** Comparison of glycoprotein composition. **(D)** Comparison of proteoglycan composition. **(E)** Comparison of other fibers in the ECM. ECM, extracellular matrix. Color images are available online.

in the longitudinal direction and in higher strain,[26,27] decellularized ECM from the apex can be reasonably expected to exert more passive stress and be stiffer at higher stretch. This understanding is consistent with our observations of the three regions of LV scaffolds.

In comparison, the three regions along the axial dimension of the tenderloin do not exhibit similar variability and instead demonstrate better passive mechanical consistency. This is consistent with classic reports of tissue consistency in skeletal muscles.[23] This observation holds true for both decellularized tenderloin scaffolds and recellularized tenderloin tissues. It is also noted that tenderloin EHTs show higher passive stress and stiffness above 3–4% stretch. Since tenderloin has greater longitudinal collagen alignment according to IHC images, and our decellularized scaffolds are always aligned in the ECM fiber longitudinal direction during production and passive stretch mechanical measurement, tenderloin can be reasonably expected to possess higher passive stress at higher strain, exactly as our data show.

Tenderloin is more readily available than porcine hearts, as it is a cut of meat that can be procured from local supermarkets, whereas organs like hearts are often sourced from a specialized butcher shop or slaughterhouse. This makes the psoas major more accessible as a resource for creating scaffolds for EHTs.

Tenderloin EHTs were highly comparable in systolic function to LV tissues. In nearly every category, tenderloin tissues have almost equivalent systolic peak force and twitch kinetic parameters to LV-based EHTs. Interestingly, tenderloin tissues exhibit significantly improved Frank-Starling behavior, as their systolic forces increase more at the same stretch percentage as LV tissues. This observation has several potential implications. First of all, it has been extensively reported that titin, a giant spring-like protein in the sarcomere, has a critical role in length-dependent activation.[28]

As a result, the higher passive mechanical profiles of tenderloin EHTs and improved Frank-Starling behavior may be partially explained by a slight switch in titin isoform expression toward N2B or titin's improved ability to modulate thin and thick filaments during stretch. Since skeletal muscle cells are larger than cardiomyocytes in both length and width,[29,30] the larger space in the tenderloin ECM after decellularization may offer a more optimal environment for immature hiPSC-CM attachment and functional maturation. Furthermore, titin is not the only protein with an effect on Frank-Starling behavior. Phosphorylation of cardiac troponin-I and cardiac myosin-binding protein-C has also been shown to have an effect on length-dependent activation and could warrant further investigation in different ECMs.[31,32]

Besides ECM structures and morphologies, ECM protein compositions also have a significant impact on hiPSC-CMs. Although both skeletal and cardiac ECM are found to express collagen type I, type III, type IV, laminin, and fibronectin,[33,34] we identify nuanced variations in these ECM protein expressions and several other differentially expressed proteins in the tenderloin and LV ECM. In comparing the tenderloin and LV ECM, we see a markedly higher type III collagen in LV, indicating and agreeing with the higher compliance seen in LV ECM passive mechanics. Our data also point to a higher type IV collagen expression in tenderloin, consistent with observations that type IV plays a role in the basement membrane for the maintenance and recovery of skeletal muscles.[35] In addition, collagen type V is present in the core of some type I collagens,[36] with LV expressing more type V than tenderloin.

It is noted that, although collagen type I is the most abundant collagen, it did not clearly show up in the mass spectrometry data. There are several possible reasons. First, unlike human and mouse proteomics database, porcine proteomic data are likely used less frequently and therefore are not as well annotated, leading to possible omission of collagen type I. In addition, mass spectrometry software relies on a bottom-up approach that predicts the protein based on the peptides found. Since collagen subtypes share high homology similarities, it is reasonable to suspect that collagen type I peptides were incorrectly categorized under other subtypes. However, given both tenderloin and LV samples were from the same species, there are unlikely significant discrepancies between the two samples' collagen analysis results.

Tenderloin and LV also share and differ in ECM glycoproteins. Fibrillin, a type of commonly expressed glycoproteins found in both tenderloin and LV ECM, is integral in a large number of extracellular, cell surface, and signaling networks and pathways that maintain morphogenetic and homeostatic functions.[37] Tenderloin ECM is found to have a higher expression of fibrillin-1. With evidence that suggests high-affinity heparin-binding site adjacent to fibrillin-1's RGD site,[38] more fibrillin-1 present in tenderloin may enhance hiPSC-CMs' integrin-mediated cell adhesion and result in improved active mechanical behavior of tenderloin EHTs.

Collectively, the mass spectrometry data reveal distinct and shared ECM protein profiles between tenderloin and LV decellularized scaffolds. Overall, tenderloin and LV showed similar total ECM protein contents, with characteristic protein expression differences across collagens, glycoproteins, proteoglycans, and other basement membrane proteins. Functionally, although tenderloin lacks or shows lower expression of some ECM proteins including collagen type III, nidogen-1, perlecan, laminin, and fibronectin, tenderloin EHTs still demonstrate highly comparable active mechanical profiles to LV tissues, suggesting that for a simplified *in vitro* tissue model studying fundamental muscle mechanics or inherited cardiomyopathy genetic mutations, tenderloin ECM may provide a more minimal, but sufficient ECM infrastructure for proper cell attachment and contractility mediation with more consistent passive mechanical properties.

Of course, there are several limitations to be acknowledged. The use of SDS is much harsher in decellularizing porcine tissue to use as scaffolds than other gentler methods that fully preserve collagens and glycosaminoglycans.[39] As described in our mass spectrometry data, there may have been loss of ECM proteins. While it may be desirable in principle to avoid any loss in the decellularization process, as a practical matter, we have found that the SDS treatment makes seeding cells into scaffolds easier than in a more delicately preserved ECM.

Although there are many other characteristics and properties to be compared between EHTs made from

decellularized porcine psoas versus porcine heart scaffolds, this study focuses primarily on the essential characteristics showcasing the similarities in biomechanical function. In previous articles by our group, EHTs made from left ventricular free wall, more extensive studies have been conducted on tissue remodeling and cell-matrix adhesion.[2,8] Although these evaluations were omitted in this particular article, since the main attributes (contractile force and twitch kinetics) have no significant difference, it is likely that the other underlying elements only have subtle changes, if any.

Regarding the maturity of our tissues, it has been previously reported that our EHTs made from hiPSC-CMs have equivalent twitches to those recorded from human ventricular trabeculae, suggesting the functionality is comparable.[2] As for the morphology and composition, human ventricular cardiomyocytes predominantly express the beta isoform of myosin heavy chain (MHC), which our group has previously shown to be consistent in our iPSC-CM-seeded EHTs.[40] Before testing active mechanics, the tissues we cultured for 2 weeks to let the stem cell-derived cardiomyocytes mature.

Through the evaluation of passive and active mechanics, porcine psoas shows promise as a functionally equivalent alternative to porcine ventricular tissue as a source for decellularized scaffolds in EHTs.

## Authors' Contributions

S.S.: Conceptualization; methodology; and writing–original draft. S.S.: Visualization; investigation; writing–original draft; and formal analysis. M.P.: Investigation; writing–original draft; and formal analysis. J.A.K.: Supervision and writing–review and editing. S.G.C.: Conceptualization; supervision; writing–review and editing; funding acquisition; and project administration.

## Disclosure Statement

S.G.C. has equity ownership in Propria LLC, which has licensed EHT technology used in the research reported in this publication. This arrangement has been reviewed and approved by the Yale University Conflict of Interest Office. The authors declare no additional competing financial interests. J.A.K. provided consulting and collaborative studies with various pharmaceutical companies, but the content of this work is unrelated to the article.

## Funding Information

We acknowledge the following sources of support: NIH R01HL136590 and NSF CAREER 1653160 to SGC; and NIH R01HL136737 to JAK.

## References

1. Jung JP, Hu D, Domian IJ, et al. An integrated statistical model for enhanced murine cardiomyocyte differentiation via optimized engagement of 3D extracellular matrices. Sci Rep 2015;5:18705; doi: 10.1038/SREP18705
2. Schwan J, Kwaczala AT, Ryan TJ, et al. Anisotropic engineered heart tissue made from laser-cut decellularized myocardium. Sci Rep 2016;6:32068.
3. Ott HC, Matthiesen TS, Goh SK, et al. Perfusion-decellularized matrix: Using nature's platform to engineer a bioartificial heart. Nat Med 2008;14:213–221.
4. Guyette JP, Charest JM, Mills RW, et al. Bioengineering human myocardium on native extracellular matrix. Circ Res 2016;118:56–72.
5. Crapo PM, Gilbert TW, Badylak SF. An overview of tissue and whole organ decellularization processes. Biomaterials 2011;32:3233–3243.
6. Zhang X, Chen X, Hong H, et al. Decellularized extracellular matrix scaffolds: Recent trends and emerging strategies in tissue engineering. Bioact Mater 2021;10:15–31.
7. Wang Y, Nicolas CT, Chen HS, et al. Recent advances in decellularization and recellularization for tissue-engineered liver grafts. Cells Tissues Organs 2017;203:203–214.
8. Sewanan LR, Schwan J, Kluger J, et al. Extracellular matrix from hypertrophic myocardium provokes impaired twitch dynamics in healthy cardiomyocytes. JACC Basic Transl Sci 2019;4:495–505.
9. Jacot JG, Martin JC, Hunt DL. Mechanobiology of cardiomyocyte development. J Biomech 2010;43:93–98.
10. Shen S, Sewanan LR, Campbell SG. Evidence for synergy between sarcomeres and fibroblasts in an in vitro model of myocardial reverse remodeling. J Mol Cell Cardiol 2021; 158:11–25.
11. Lian X, Zhang J, Azarin SM, et al. Directed cardiomyocyte differentiation from human pluripotent stem cells by modulating Wnt/β-catenin signaling under fully defined conditions. Nat Protoc 2013;8:162–175.
12. Ng R, Manring H, Papoutsidakis N, et al. Patient mutations linked to arrhythmogenic cardiomyopathy enhance calpain-mediated desmoplakin degradation. JCI insight 2019;5(14): e128643; doi: 10.1172/JCI.INSIGHT.128643
13. Sewanan LR, Campbell SG. Modelling sarcomeric cardiomyopathies with human cardiomyocytes derived from induced pluripotent stem cells. J Physiol 2020;598:2909–2922.
14. Sewanan LR, Shen S, Campbell SG. Mavacamten preserves length-dependent contractility and improves diastolic function in human engineered heart tissue. Am J Physiol Heart Circ Physiol 2021;320:H1112–H1123.
15. Shen S, Sewanan LR, Jacoby DL, et al. Danicamtiv enhances systolic function and frank-starling behavior at minimal diastolic cost in engineered human myocardium. J Am Heart Assoc 2021;10(12):e020860; doi: 10.1161/JAHA.121.020860
16. Bekhite MM, Schulze PC. Human induced pluripotent stem cell as a disease modeling and drug development platform-a cardiac perspective. Cells 2021;10:3483.
17. Lelovas PP, Kostomitsopoulos NG, Xanthos TT. A comparative anatomic and physiologic overview of the porcine heart. J Am Assoc Lab Anim Sci 2014;53:432.
18. Reardon S. First pig-to-human heart transplant: What can scientists learn? Nature 2022;601(7893):305–306; doi: 10.1038/D41586-022-00111-9
19. Salvatori M, Peloso A, Katari R, et al. Semi-xenotransplantation: The regenerative medicine-based approach to immunosuppression-free transplantation and to meet the organ demand. Xenotransplantation 2015;22:1–6.
20. Streeter DD, Spotnitz HM, Patel DP, et al. Fiber orientation in the canine left ventricle during diastole and systole. Circ Res 1969;24:339–347.
21. Rabben SI, Irgens F, Angelsen B. Equations for estimating muscle fiber stress in the left ventricular wall. Heart Vessels 1999;14:189–196.

22. Dorado M, Martín Gómez EM, Jiménez-Colmenero F, et al. Cholesterol and fat contents of Spanish commercial pork cuts. Meat Sci 1999;51:321–323.
23. Farrell PR, Fedde MR. Uniformity of structural characteristics throughout the length of skeletal muscle fibers. Anat Rec 1969;164:219–229.
24. Didangelos A, Yin X, Mandal K, et al. Extracellular matrix composition and remodeling in human abdominal aortic aneurysms: A proteomics approach. Mol Cell Proteomics 2011;10(8):M111.008128; doi: 10.1074/MCP.M111.008128
25. Patterson NL, Iyer RP, de Castro Brás LE, et al. Using proteomics to uncover extracellular matrix interactions during cardiac remodeling. Proteomics Clin Appl 2013;7:516–527.
26. Granzier HL, Irving TC. Passive tension in cardiac muscle: Contribution of collagen, titin, microtubules, and intermediate filaments. Biophys J 1995;68:1027–1044.
27. Fu L, Ruan Q, You Z, et al. Investigation of left ventricular strain and its morphological basis during different stages of diastolic and systolic dysfunction in SHR. Am J Hypertens 2022;35(5):423–432; doi: 10.1093/AJH/HPAC008
28. Kawai M, Jin JP. Mechanisms of Frank-Starling law of the heart and stretch activation in striated muscles may have a common molecular origin. J Muscle Res Cell Motil 2021;42:355–366.
29. Litviňuková M, Talavera-López C, Maatz H, et al. Cells of the adult human heart. Nat 2020;588:466–472.
30. Alberts B, Johnson A, Lewis J, et al. Genesis, Modulation, and Regeneration of Skeletal Muscle. Available from: https://www.ncbi.nlm.nih.gov/books/NBK26853/[Last accessed: February 1, 2022].
31. Rao VS, Korte FS, Razumova MV, et al. N-terminal phosphorylation of cardiac troponin-I reduces length-dependent calcium sensitivity of contraction in cardiac muscle. J Physiol 2013;591:475–490.
32. Hanft LM, Fitzsimons DP, Hacker TA, et al. Cardiac MyBP-C phosphorylation regulates the Frank-Starling relationship in murine hearts. J Gen Physiol 2021;153(7):e202012770; doi: 10.1085/JGP.202012770
33. Macfelda K, Kapeller B, Wilbacher I, et al. Behavior of cardiomyocytes and skeletal muscle cells on different extracellular matrix components—relevance for cardiac tissue engineering. Artif Organs 2007;31:4–12.
34. Hong X, Yuan Y, Sun X, et al. Skeletal extracellular matrix supports cardiac differentiation of embryonic stem cells: A potential scaffold for engineered cardiac tissue. Cell Physiol Biochem 2018;45:319–331.
35. Kanazawa Y, Nagano M, Koinuma S, et al. Effects of endurance exercise on basement membrane in the soleus muscle of aged rats. Acta Histochem Cytochem 2021;54:167–175.
36. Pinkert MA, Hortensius RA, Ogle BM, et al. Imaging the cardiac extracellular matrix. Adv Exp Med Biol 2018;1098:21.
37. Ramirez F, Sakai LY. Biogenesis and function of fibrillin assemblies. Cell Tissue Res 2010;339:71–82.
38. Bax DV, Mahalingam Y, Cain S, et al. Cell adhesion to fibrillin-1: Identification of an Arg-Gly-Asp-dependent synergy region and a heparin-binding site that regulates focal adhesion formation. J Cell Sci 2007;120:1383–1392.
39. Gillies AR, Smith LR, Lieber RL, Varghese S. Method for decellularizing skeletal muscle without detergents or proteolytic enzymes. Tissue Eng Part C Methods 2011;17(4):383–389.
40. Ng R, Sewanan LR, Stankey P, Li X, Qyang Y, Campbell S. Shortening velocity causes myosin isoform shift in human engineered heart tissues. Circ Res 2021;128(2):281–283.

Address correspondence to:
*Stuart G. Campbell, PhD*
*Department of Biomedical Engineering*
*Yale University*
*55 Prospect Street, MEC 211*
*New Haven, CT 06511*
*USA*

*E-mail:* stuart.campbell@yale.edu

*Received: April 3, 2023*
*Accepted: July 10, 2023*
*Online Publication Date: August 11, 2023*